

PAPER • OPEN ACCESS

Printing Parameter Optimization of Biodegradable PLA Stent Strut Thickness by using Response Surface Methodology (RSM)

To cite this article: Amirul Asyraf Azli *et al* 2020 *IOP Conf. Ser.: Mater. Sci. Eng.* **864** 012154

View the [article online](#) for updates and enhancements.

You may also like

- [3D printed auxetic stents with re-entrant and chiral topologies](#)
Amer Alomarah, Zahraa A Al-Ibraheemi and Dong Ruan
- [First heating measurements of endovascular stents in magnetic particle imaging](#)
Franz Wegner, Thomas Friedrich, Nikolaos Panagiotopoulos *et al.*
- [Design and fabrication of novel polymeric biodegradable stents for small caliber blood vessels by computer-aided wet-spinning](#)
D Puppi, A Piroso, G Lupi *et al.*



ECS
The
Electrochemical
Society
Advancing solid state &
electrochemical science & technology

DISCOVER
how sustainability
intersects with
electrochemistry & solid
state science research

Printing Parameter Optimization of Biodegradable PLA Stent Strut Thickness by using Response Surface Methodology (RSM)

Amirul Asyraf Azli¹, Noorhafiza Muhammad^{1,2}, Mohd Mustafa Abdullah Albakri², Mohd Fathullah Ghazali^{1,2}, Shayfull Zamree Abd Rahim^{1,2} and Sandu Andrei Victor^{2,3}

¹School of Manufacturing Engineering, Pauh Putra Main Campus, Universiti Malaysia Perlis, Jalan Arau-Changlun, 02600, Arau, Perlis, Malaysia

²Center of Excellence Geopolymer and Green Technology (CEGeoGTech), School of Materials Engineering, Universiti Malaysia Perlis (UniMAP), Perlis, Malaysia

³Faculty of Materials Science and Engineering, Gheorghe Asachi Technical University of Iasi, Str. D. Mangeron 41, Iasi, Romania

E-mail: noorhafiza@unimap.edu.my

Abstract. This work presents printing parameter optimization of 3D printed biodegradable PLA stent. This study is motivated by a gap in current knowledge in 3D printing of stents identified in an extensive literature review. With the demand of coronary artery stents rising every year, the stent production demands a higher quality, lower cost, faster and economical process. Due to its availability relatively low-cost price and adaptability, PLA has been identified for an ideal material for biodegradable stents. Previously, laser micromachining was widely used for processing coronary stent. The emerging of 3D printing process has gained attention for its low cost, high reliability, simple operation and flexibility has shown potential as promising solutions in stents fabrication. The use of 3D printing for stent manufacturing purpose is newly emerge and not widely reported. Up to now, less research has been conducted on 3D printed PLA coronary artery stents. This work therefore, aims to study the relationship of the 3D printing processing parameter towards stents quality. Strut thickness become the key aspects in stents manufacturing. Processing parameter optimization was performed by using Response Surface Methodology (RSM). Nozzle temperature and printing speed were both effecting the strut thickness formations regardless of printing orientations.

1. Introduction

Three-dimensional printing (3D printing), also termed additive manufacturing, relates directly to produce from virtual models of three-dimensional objects [1,2]. It is a method whereby digital 3D design information are used starting from drawing the model in any (CAD) Professional Software such as SolidWorks, CATIA and Inventor followed by slicing the model layer-by-layer to generate the GCode and finally depositing material to form the part. It has been widely optimized during this period of industrial revolutions in aeronautical, automotive, food, medical, electronic and other industries [3,4].

3D printing of coronary stents for the treatment of coronary artery disease is one of the newly emerged applications in the additive manufacturing in biomedical engineering. Stent is a wire mesh tube that opens the artery and is permanently left there. Coronary artery stenting was the preferred treatment



for patients with coronary angioplasty conditions where stent can improve their chances of survival more than thrombolytic drugs when they have a heart attack. The surgery may also reduce the likelihood of a future heart attack.

A wide range of biodegradable materials have been used in medical applications specifically in coronary artery stent, ranging from metals to polymers. The antithrombotic effect of the generated electronegative charge from erosion has been demonstrated in recent studies of Magnesium Alloy based stents [5]. The stiffness of the stent is steadily reduced by surface erosion; the radial force may be decreased early in just a few days, even if the stiffness is not fully eroded until day 60. In contrast, polymeric based materials such as Polylactic acid (PLA) is ideal for the usage in a range of medical implants at utmost importance owing to its biocompatibility, full biodegradability and the non-toxic nature of degradation products [6].

By far, the vast majority of coronary stents are produced by laser cutting from tubing materials. However, structuring such delicate stent structure especially with polymeric based materials would be very challenging by using laser cutting. Of late, 3D printing has emerged and offers alternative system for producing stent. Fused Deposition Modelling (FDM), one sort of 3D printing technologies, has gained attention for its low cost, high reliability, simple operation & personal designing. The use of 3D printing for stent purpose is newly emerge and not widely reported. Up to now, a very little research has been conducted particularly on PLA 3D printing of coronary artery stents. This work therefore aims to understand the fundamental behind the correlation between the 3D printing process parameters towards the stent strut thickness. Strut thickness uniformity ensure the stent hold in position and have sufficient strength to open the blockage vessels. On the other hand, high dimensional accuracy shows massive deliverability and help to reduce the risk of restenosis.

2. Methodology

2.1 The Stent Design

CATIA V5 software was used to design the stent profile and geometry for the 3D printing process. Figure 1 shows the 2D stent geometry and figure 2 shows the 3D model of the stent design that was used in this experiment. Figure 3 shows the stent characterizations and the detailed dimension were represented in table 1.

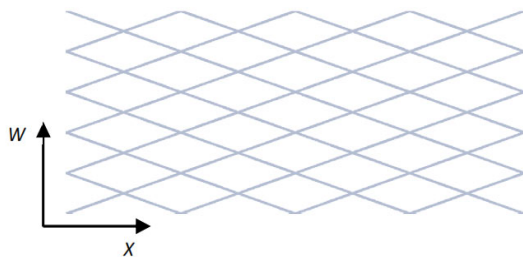


Figure 1. Stent Geometry

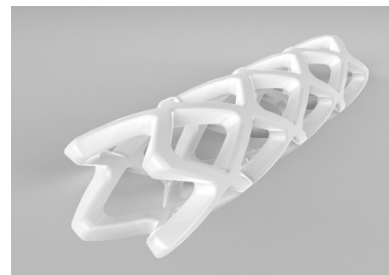


Figure 2. PLA Stent 3D Model

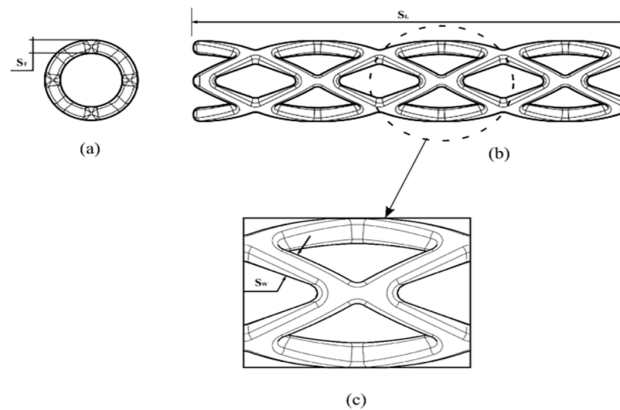


Figure 3. Stent Characterizations (a) Strut Thickness
(b) Stent Length (c) Strut Width

Table 1. Stent Dimensions

Stent Length, S_L	Strut Thickness, S_T	Strut Width, S_W
14 mm	1 mm	1 mm

2.2 Materials

In this work, Polylactic acid (PLA) was used. Polymeric based materials such as Polylactic acid (PLA) are ideal for the usage in a range of medical implants at utmost importance owing to its biocompatibility, full biodegradability, the non-toxic nature of degradation products. Upon degradation, it is important for the product to reabsorb or eradicated from the body. Table 2 shows the physical properties of PLA and table 3 shows the PLA filament specifications.

Table 2. PLA Physical Properties [7]

Materials	Tensile Strength (MPa)	Young's Modulus (GPa)	Elongation (%)	Degradation Time
PLA	60-70	108	3.75	≈12 months

Table 3. PLA Filament Specifications

Materials	Diameter (mm)	Print Temperature (°C)	Bed Temperature (°C)	Weight (kg)
PLA	1.75 ± 0.05	190 ~ 210	30 ~ 50	1.0

2.3 The FDM 3D Printer

The FDM 3D Printer, Creality Ender 3 Pro with 0.4 mm nozzle diameter was used in this work. The Computer Aided Design (CAD) data of the stent design was created (figure 2) and transferred to the 3D Printer machine. The data were translated into G-code programming by the computer system which enables one to perform the printing process with the desired geometric and dimension. The PLA filaments were printed in X, Y and Z directions. Figure 4 illustrates the schematic diagram of FDM 3D printer.

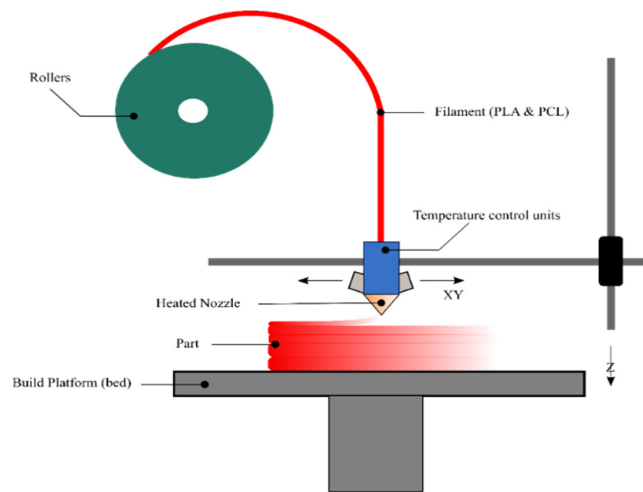


Figure 4. FDM 3D Printer Schematic Diagram

2.4 Response Surface Methodology (RSM) and Central Composite Design (CCD)

The studied printing parameters were printing orientations, nozzle temperature and printing speed. Response Surface Methodology (RSM) and Central Composite Design (CCD) was the statistical techniques selected to optimize the processing parameters of FDM 3D printed of coronary artery stents. Table 4 shows the factors and level for this research which was developed using Minitab 19 software.

Table 4. Process Parameters and Levels

Continuos Factors				
Factor	Process Parameter	Unit	Low Level (-1)	High Level (+1)
A	Printing speed	mm/s	3	10
B	Nozzle Temperature	$^{\circ}\text{C}$	190	220
Categorical Factors				
Factor	Process Parameter	Levels	Level values	
C	Printing orientations	2	(1) XY	(2) ZX

The factors divided into two types which is continuous and categorical factors. Printing speed and nozzle temperature have been categorized as continuous factors as they have binary quantities of infinite numbers of two values. Printing orientation is categorized as categorical factors because the values were not numerical and it described data that fits into categories. 26 experiments were performed based on the design of experiment, (DOE) generated from Minitab 19 software randomly.

The printing parameters that were kept constant during the experiment are shown in *Table 5*. Room temperature of the laboratory was 20°C .

Table 5. Constant Printing Parameters

Parameters	Unit	Values
3D accuracy resolution	μm	0.01
Layer height	mm	0.2
Infill density	%	0

In standard RSM approaches, the variables should be continuous and no variables can be categorical [8-11]. Thus, in this research, two-factor factorial experiment with comparing two different types of printing orientations has been considered in order to get the comparisons data within these two categorical inputs.

In this work, full central composite design for optimization of two variables was used. For two continuous variables, α -values can be calculated by $\alpha = (2^2)^{1/4}$ or $\alpha = 1.41421$ [12]. All factors in full uniformly routable central composite designs are studied in five levels ($-\alpha$, -1 , 0 , 1 and α) [13].

3. Results and discussions

3.1 Experimental Results

The results of the strut thickness have been obtained from the experimental work. It was processed in the Minitab 19 Software to determine the influence of the printing orientation, nozzle temperature and printing speed towards the strut thickness. The results were obtained from the 26 samples. Table 6 shows the results of the strut thickness dimension. Surface Regression Methodology (RSM) was applied to assess the statistical significance for strut thickness influenced by the printing parameters. The analysis was conducted at a confidence level of 95% ($\alpha = 0.05$) with one replicate [14-15]. Table 7 shows the Axial Point Data Effects of strut thickness.

Table 6. Experimental Results of strut thickness

Run #	P _s (mm/s)	N _T (°C)	P _o (axis)	S _T (mm)
1	10	190	XY	0.95
2	10	220	XY	1.2
3	6.5	205	ZX	1.26
4	6.5	205	XY	1.16
5	3	190	ZX	1.2
6	3	190	XY	1.08
7	10	190	ZX	1.13
8	6.5	205	ZX	1.28
9	6.5	226.213	ZX	1.14
10	6.5	205	ZX	1.29
11	11.4497	205	ZX	1.12
12	6.5	205	ZX	1.28
13	6.5	226.213	XY	1.1
14	3	220	ZX	1.66
15	6.5	205	XY	1.18
16	1.55025	205	XY	0
17	6.5	205	XY	1.14
18	6.5	183.787	XY	0.98
19	11.4497	205	XY	1.01
20	3	220	XY	1.67
21	6.5	205	XY	1.14
22	6.5	205	XY	1.1
23	1.55025	205	ZX	1.2
24	6.5	183.787	ZX	1.11
25	6.5	205	ZX	1.29
26	10	220	ZX	1.25

Axial point data is the mean of both upper and lower level $\pm \alpha$ (range between the upper and lower level divided by 2). It shows the effects of factors when it goes beyond or below the experimental factors range. One can clearly see the results that strut thickness only shows negative effects when the printing speed way below the range of experimental factors which is at 1.55025 mm/s. As the deposited materials bridging on the next layer with slowest printing speed, the heat generated directed down the tip of the nozzle head actually reheating back the previous layer making it a partial liquid form. Thus, making the previous solidified layer clotting to the nozzle tip. Referring to Conduction of Heat equation in equation 1, knowing that Q represents the amount of heat transferred in a time, t; the lower the value of t, the higher the conduction of heat produce by the nozzle through the solidified layers.

Table 7. Axial Point Data Effects of strut thickness

Samples #	P _s	N _T	P _O	S _T
9	6.5	226.213	ZX	1.14
13	6.5	226.213	XY	1.1
18	6.5	183.787	XY	0.98
24	6.5	183.787	ZX	1.11
11	11.4497	205	ZX	1.12
19	11.4497	205	XY	1.01
16	1.55025	205	XY	0
23	1.55025	205	ZX	1.2

$$Q/t = kA\Delta T/d \tag{1}$$

Where;

Q/t = Amount of heat transferred in a time, t (Watts)

k = thermal conductivity constant for the material

A = cross sectional area of the material transferring heat (mm²)

ΔT = difference in temperature between one side of the material and the other (°C)

d = thickness of the material (mm)

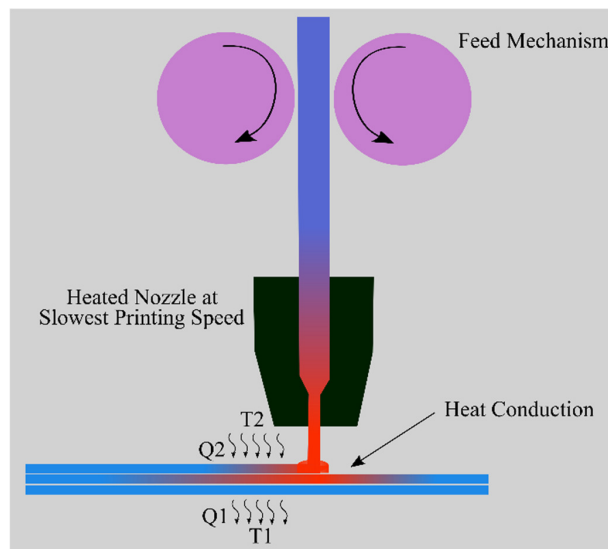


Figure 5. Heat Conduction of Nozzle Head

The heat conduction phenomenon develop by the nozzle head were clearly shown in figure 5. Both samples 18 and 24 were printed with nozzle temperature that was below the recommended print temperature of PLA filament. Due to that conditions, the extruded filament widths for the samples 18 and 24 were considerably smaller compared to those fabricated between 190 °C to 220 °C which consequently resulted in significantly bigger air gaps for the samples fabricated below the recommended print temperature of PLA filament.

3.2 ANOVA of Strut Thickness

The result of ANOVA for strut thickness is presented in table 8. The null hypothesis, HO stated that there is no relationship between the 3D printing processing parameters and strut thickness. From the ANOVA results, the p-value is less than 0.05 which mean that the model term is statistically significant at 95% Confidence Interval (CI). It also indicates strong evidence against the null hypothesis. Thus, the null hypothesis was rejected. In this case study, printing speed and nozzle temperature are significant model terms. R-Sq co-efficient is the ratio of explained variability to the total variability in the actual data and the model is perfectly fit for the actual data when this value is proximate to unity. From the calculated R-Sq value of 0.7279 in table 9 is understood that the quadratic strut thickness model can be explained the variation up to the extent of 72.79% respectively. The R-Sq(adj) values are noticed that the relationship between the input 3D printing processing parameters and the stent length describes by proposed model. R-Sq(adj) value of 0.2924 is reasonable agreed. These results also indicate that printing orientation does not improve the strut thickness model. Hence, from the result analysis obtained, as shown in table 9, the most significant factor affecting the strut thickness is printing speed. The regression equations for strut thickness in equation 2 and 3 are obtained by the regression analysis of the data in table 10.

Table 8. Analysis of Variance (ANOVA) of Strut Thickness

Source	DF	Adj SS	Adj MS	F	P
Model	8	0.639286	0.079911	5.02	0.004
Linear	3	0.427564	0.142521	8.95	0.001
A – Printing Speed, Ps	1	0.240100	0.240100	15.07	0.001
B – Nozzle Temp, NT	1	0.187171	0.187171	11.75	0.004
C – Print Orientations, Po	1	0.000294	0.000294	0.02	0.894
Square	2	0.119644	0.059822	3.76	0.048
Ps ²	1	0.107494	0.107494	6.75	0.020
NT ²	1	0.012150	0.012150	0.76	0.396
2-Way Interaction	3	0.114411	0.038137	2.39	0.109
Ps * NT	1	0.044592	0.044592	2.80	0.115
Ps * Po	1	0.049539	0.049539	3.11	0.098
NT* Po	1	0.020280	0.020280	1.27	0.277
Error	17	0.238964	0.015931		
Lack-of-Fit	9	0.238183	0.029994	271.07	0.000
Pure Error	8	0.000781	0.000011		
Total	25				

Table 9. Adequacy of the Strut Thickness Model

Standard Deviations	R-Sq (%)	R-Sq(adj) (%)
0.1262	0.7279	0.292

Table 10. Coefficients Table for Strut Thickness Fit Regression Model

Term	Coef	SE Coef	T-Value	P-Value
Constant	-10.9	10.9	-1.00	0.332
A – Printing Speed, P _S	0.043	0.177	0.24	0.810
B – Nozzle Temp, N _T	0.109	0.106	1.03	0.320
C – Print Orientations, P _o				
XY	-0.436	0.476	-0.92	0.374
ZX	0.436	0.476	0.92	0.374
P _S ²	0.01463	0.00563	2.60	0.020
N _T ²	-0.000225	0.000258	-0.87	0.396
P _S * N _T	-0.001310	0.000783	-1.67	0.115
P _S * P _o				
XY	-0.01543	0.00875	-1.76	0.098
ZX	0.01543	0.00875	1.76	0.098
N _T * P _o				
XY	0.00260	0.00230	1.13	0.277
ZX	-0.00260	0.00230	-1.13	0.277

$$ST(xy) = -11.3 + 0.028 PS + 0.111 NT + 0.01463 (PS)^2 - 0.000225 (NT)^2 - 0.001310 (PS)(NT) \quad (2)$$

$$ST(zx) = -10.4 + 0.059 PS + 0.106 NT + 0.01463 (PS)^2 - 0.000225 (NT)^2 - 0.001310 (PS)(NT) \quad (3)$$

These equations give optimized value for all process parameters which will yield the best possible strut thickness at two different type of printing orientations and at any value of printing speed and nozzle temperature.

3.3 Response Surface Methodology (RSM) for strut thickness

The normal probability plot for residuals graph in figure 6(a) shows that errors are distributed normally since the residuals fall on the straight line. Based on standardize effects plot on Figure 6(b), the effects of printing orientation did not show a clear tendency. It was found that orientation in printing would not affects the strut thickness dimension. From the surface and contour plot shown in figure 7, it can be observed that minimum pattern surface plot was obtained on both printing orientation. Based on figure 7(a)(b) thicker strut thickness form a ridge running on upper left of the graph. The valleys from the upper middle to the lower right of the graph represent nozzle temperature and printing speed combinations that result in thinner strut thickness which indicated the best quality of stent characterizations. With an increase in nozzle temperature, strut thickness will increase rapidly. Meanwhile, on figure 7(c)(d) it shows slightly different results on ZX - orientations. Thicker strut thickness seems to form a ridge running on upper left and middle right of the graph. By changing the build orientation to ZX, thicker strut formations not only occur due to nozzle temperature but with an increase in printing speed, strut thickness are increase initially and decrease slightly until the middle valley ranging (5-8 mm/s). The strut thickness starts to increase again when the printing speed is out from the range.

Printing orientation does not have a major influence on the thickness of the strut but the printing speed has a significantly bigger effect on the strut thickness. Strut thickness decreases as printing speed increases. However, unsuitable printing speed with low nozzle temperature will contribute to imperfect stent formation, since the deposited filament will not stick to the printing bed and the printed layer

becomes disorderly. This is because when filaments were not fully melted by the heater, the material fails to be deposited in line with the printing speed.

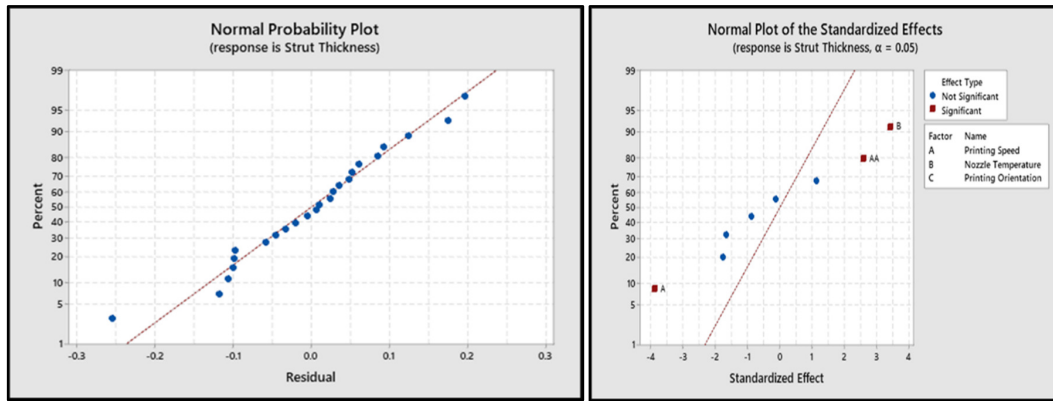


Figure 6. (a) Normal Probability Plot for Residual of ST Data (b) Normal Plot of Standardized Effects ST Data

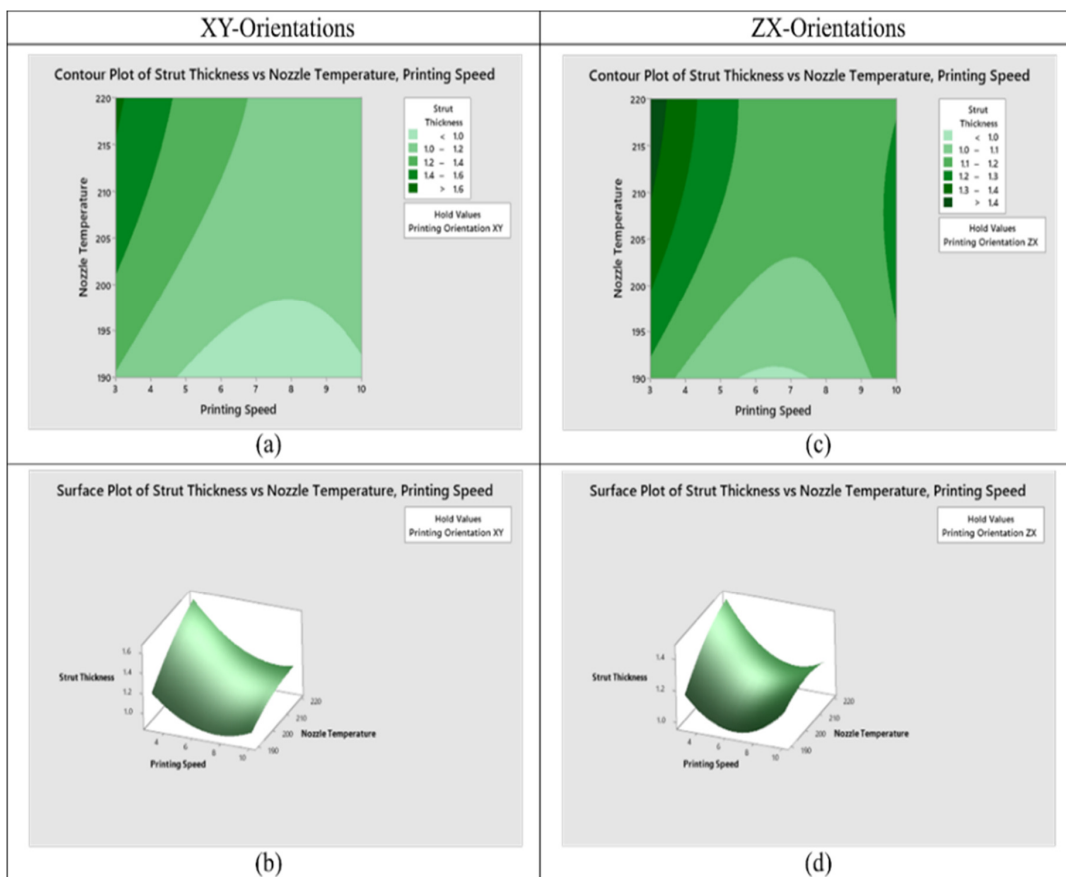


Figure 7. XY – Orientation Contour Plot (a) Surface Plot (b) ZX – Orientation Contour Plot (c) Surface Plot (d) of Strut Thickness vs Nozzle Temperature, Printing Speed

3.4 Validation

To validate the current strut thickness model, the simulation results were compared against experimental data by response optimizations approach. The optimum range of input parameter setting and the corresponding output response value are as shown in table 11 and 12. From table 13, it was clear that absolute error between the experimental value and the predicted value lie within 6%. Thus, this model could be efficiently used to predict the input parameters during 3D printing process of PLA coronary artery stents. Figure 8 shows the 3D printed PLA stents using the optimized strut thickness parameters.

Table 11. Strut thickness response optimizations parameters

Response	Goal	Lower	Target	Upper	Weight	Importance
Strut Thickness	Target	0.9	1	1.1	1	1

Table 12. Strut thickness multiple response prediction

Variable	Setting			
Printing speed	4.72613			
Nozzle	190			
Temperature				
Printing orientation	XY			
	Fit	SE Fit	95% CI	95% PI
Strut thickness	1.00	0.0757	(0.8386,1.1614)	(0.6862, 1.3138)

Table 13. Optimum ST Result of RSM

Response	Goal	Predicted Value	Experimental Value	Error(%)
Strut Thickness(mm)	Targeted	1.0	0.94	6

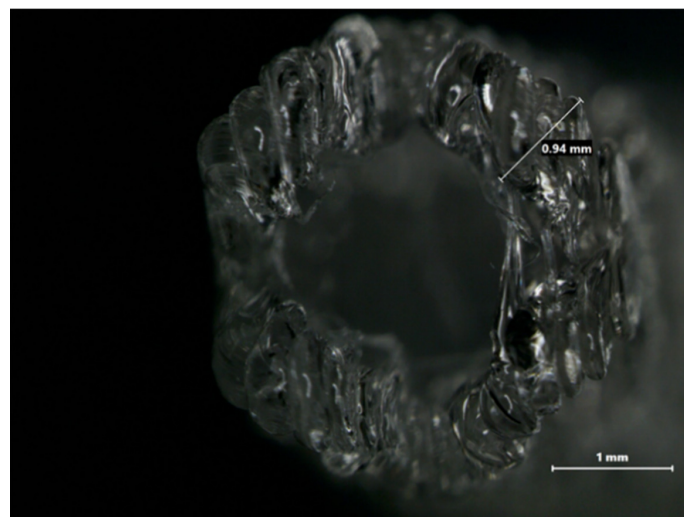


Figure 8. PLA Stent with Optimized Parameters for Strut Thickness Under Low Power Microscope

4. Conclusion

The effects of 3D printing process parameters (printing orientation, nozzle temperature and printing speed) had been clearly discussed to support the experimental findings in this research works in terms of dimensional accuracy of coronary artery stents strut thickness. Overall findings, the nozzle temperature and printing speed play the important role in affecting the dimensional accuracy of strut thickness. This is because the inclination of nozzle temperature, with a low printing speed drastically increase the strut thickness, compared to printing orientations effects.

XY-printing orientations is the ideal printing orientation for 3D printed PLA stents as it provides good dimensional precision for stent characterizations and a lower risk for the structure and geometry to be sagging during the printing process. The gravitational force of 3D printed stent on XY-printing orientations is minimized by lowering the centre of gravity (COG) compared to ZX-orientations. The optimum 3D printing processing parameters for PLA coronary artery stents are shown in Table 14. Room temperature also need to be considered as it will affect the heated nozzle temperature. This experimental works is conducted in 20 °C laboratory.

Table 14. Optimum FDM Stent 3D Printing Processing Parameters

Factor	Process Parameter	Unit	Value/Range
A	Printing Speed	mm/s	4.5 -5
B	Nozzle Temperature	°C	190
C	Printing Orientation	-	XY

References

- [1] Santos K, Loures E, Piechnicki F and Canciglieri O 2017 *Procedia Manuf.* **11** p 1358
- [2] Radhwan H, Shayfull Z, Abdellah A E-H, Irfan A R and Kamarudin K 2019 *AIP Conf. Proc.* **2129** p 020154
- [3] Shahrubudina N, Leea T C and Ramlana R 2019 *Procedia Manuf.* **35** p 1286
- [4] Radhwan H, Shayfull Z, Farizuan M R, Effendi M S M and Irfan A R 2019 *AIP Conf. Proc.* **2129** p 020158
- [5] Hyuk Im S, Jung Y and Kim S H 2019 *Mater. Sc. Eng.* **99** p 1274
- [6] Rajendra P Pawar, Sunil U Tekale, Suresh U Shisodia, Jalinder T Totre and Abraham J Domb 2014 *Recent Patents on Regenerative Medicine* **4** p 40-51
- [7] Guerra A J, Paula Cano, Rabionet M, Puig T and Ciurana J 2018 *Materials* **11** p 1679
- [8] M Isafiq, Z Shayfull, S M Nasir, M M Rashidi, M Fathullah and N Z Noriman 2016 *MATEC Web of Conferences.* **78** 01084
- [9] Allen and Theodore T 2006 (London: Springer Publishers)
- [10] S M Nasir, K A Ismail and Z Shayfull 2016 *Key Engineering Materials.* **700** 12-21
- [11] Radhwan H, Shayfull Z, Farizuan M R, Effendi M S M and Irfan A R 2019 *AIP Conf. Proc.* **2129** p 020155
- [12] Douglas C Montgomery, George C Runger 2003 (New York: John Wiley & Sons, Inc. Publishers) p. 505
- [13] Bezerra M A, Santelli R E, Oliveira E P, Villar L S and Escaleira L A 2008 *Talanta* **76** p 9656
- [14] J M Faiz, Z Shayfull, S M Nasir, M Fathullah and M M Rashidi 2017 *AIP Conference Proceedings.* **1885** 020071
- [15] N Rayhana, M Fathullah, Z Shayfull, S M Nasir, M H M Hazwan, M Sazli and Z. R. Yahya 2017 *AIP Conference Proceedings.* **1885** 020097